Photochemical Haze Formation in the Atmospheres of super-Earths and mini-Neptunes

Chao He[1], Sarah M. Hörst[1], Nikole K. Lewis[1,2], Xinting Yu[1], Julianne I. Moses[3], Eliza M.-R. Kempton[4], Mark S. Marley[5], Patricia McGuiggan[6], Caroline V. Morley[7], Jeff A. Valenti[2], & Véronique Vuitton[8]

[1] Department of Earth and Planetary Sciences, Johns Hopkins University, Baltimore, MD, USA che13@jhu.edu

[2]Space Telescope Science Institute, Baltimore, MD, USA

[3]Space Science Institute, Boulder, CO, USA

[4]Grinnell College, Grinnell, IA, USA

[5]NASA Ames Research Center, Mountain View, CA, USA

[6]Department of Materials Science and Engineering, Johns Hopkins University, Baltimore, MD, USA

[7]Harvard University, Cambridge, MA, USA

[8]Université Grenoble Alpes, Grenoble, FR

Submitted to AAS Journal

Abstract:

UV radiation can induce photochemical processes in the atmospheres of exoplanet and produce haze particles. Recent transmission spectra of super-Earths and mini-Neptunes have demonstrated the possibility that exoplanets have haze/cloud layers at high altitudes in their atmospheres. Haze particles play an important role in planetary atmospheres because they affect the chemistry, dynamics, and radiation flux in planetary atmospheres, and may provide a source of organic material to the surface which may impact the origin or evolution of life. However, very little information is known about photochemical processes in cool, high-metallicity exoplanetary atmospheres. We present here photochemical haze formation in laboratory simulation experiments with UV radiation; we explored temperatures ranging from 300 to 600 K and a range of atmospheric metallicities (100×, 1000×, and 10000× solar metallicity). We find that photochemical hazes are generated in all simulated atmospheres, but the haze production rates appear to be temperature dependent: the particles produced in each metallicity group decrease as the temperature increases. The images taken with an atomic force microscope (AFM) show that the particle size (15 nm to 190 nm) varies with temperature and metallicity. Our results provide useful laboratory data on the photochemical haze formation and particle properties, which can serve as critical inputs for exoplanet atmosphere modeling, and guide future observations of exoplanets with the Transiting Exoplanet Survey Satellite (TESS), the James Webb Space Telescope (JWST), and the Wide-Field Infrared Survey Telescope (WFIRST).

1. INTRODUCTION

Super-Earths and mini-Neptunes (generally any planet with size or mass between Earth's and Neptune's) are the most abundant types of planets among the ~3500 confirmed exoplanets (e.g., Borucki et al. 2011, Fressin et al. 2013). The atmospheres of these types of exoplanets are expected to span a large range of compositions (e.g., Elkins-Tanton & Seager 2008, Miller-Ricci et al. 2009, Schaefer et al. 2012, Moses et al. 2013, Hu & Seager 2014, Venot et al. 2015, Ito et al. 2015). The Transiting Exoplanet Survey Satellite (TESS) mission will further increase the number of super-Earths and mini-Neptunes that will be amenable to atmospheric characterization by the James Webb Space Telescope (JWST), as well as other large ground-based and space-based telescopes in the future. The TESS mission (Sullivan et al., 2015) will target stars that are 10-100 times brighter than those targeted with the Kepler mission; three-quarters of the stellar planetary hosts will be M-dwarfs, and the most planets orbiting M-dwarfs will have equilibrium temperatures (T_{eq}) <1000 K. The atmospheres of a number of small planets ($R_p < R_{Neptune}$) with cool temperatures (T_{eq} <1000 K) have now been observed, and a majority of these planets show evidence for aerosols (clouds or hazes) (e.g., Kreidberg et al. 2014; Knutson et al. 2014a, 2014b; Dragomir et al. 2015). Condensate cloud and photochemical haze particles are present in many solar system atmospheres. They are also expected in exoplanet atmospheres based on our understanding of particle formation in planetary atmospheres.

Particles play an important role in planetary atmospheres because they affect the chemistry, dynamics, and radiation flux in planetary atmospheres, and can therefore influence surface temperature and habitability. Photochemically generated hazes may provide a source of organic material to the surface which may impact the origin or evolution of life. The photochemistry induced by UV photons is universal in planet systems. Solar UV photons drive the photochemistry in atmospheres of solar system bodies (such as Venus, Earth, Jupiter, Saturn, Titan, Triton, and Pluto), and stellar UV radiation also induces photochemistry in the atmospheres of exoplanets. Studies show that the UV radiation around M dwarf planet hosts covers both far UV and near UV wavelengths; thus inclusion of UV driven atmospheric chemistry is important for

understanding atmospheres of planets orbiting most M dwarfs (e.g., France et al. 2013). Photochemistry is likely to play a major part in the atmospheres of planets with T_{eq} <1000 K, especially for super-Earths and mini-Neptunes that may have enhanced atmospheric metallicity (Marley et al. 2013). Metallicity (Z) is defined as the fractional percentage of the chemical elements other than hydrogen and helium in a star or other object (solar metallicity, Z_{sun}=0.0134). However, we currently have very little information about photochemical processes in these cool, metal-rich planetary atmospheres. Laboratory production and analysis of exoplanet hazes are essential for interpreting future spectroscopic observations and properly characterizing the atmospheres of these worlds. Recently, we reported the haze formation and particles size distribution in our plasma experiments (He et al. 2018, Hörst et al. 2018a) that probe a broad range of atmospheric parameters relevant to super-Earths and mini-Neptunes. Here, we present our investigation on photochemical haze formation by using UV radiation as energy source. We show that photochemical hazes are generated in these diverse atmospheres, and the haze production rate and the particle size varies with temperature and metallicity.

2. MATERIALS AND EXPERIMENTAL METHODS

2.1. Haze Production Setup

Figure 1 shows a schematic of Planetary Haze Research (PHAZER) experimental setup at Johns Hopkins University (He et al. 2017, 2018; Hörst et al. 2018a). The initial gas mixtures for our experiments are calculated from the chemical equilibrium models of Moses et al. (2013), who examined the possible thermochemistry and photochemistry in the atmospheres of Neptune-sized and sub-Neptune-sized exoplanets. The equilibrium calculations relevant to this investigation were performed at conditions of 300, 400, and 600 K at 1 mbar for 100×, 1000×, and 10000× solar metallicity. These high-metallicity chemical equilibrium models provide the initial conditions for our study, ensuring that the pressure, temperature, and gas compositions used in the experiments are self-consistent. As listed in Table 1, only gases with a calculated abundance of 1% or higher are included to maintain a manageable level of experimental complexity; this resulted in

no nitrogen-bearing species in two cases and the exclusion of sulfur-bearing species. Other, lower abundance species not included in these experiments (e.g., Na_2S, KCl) will condense in this temperature range and could serve as condensation nuclei.

The procedure for preparing the gas mixtures can be found in He et al (2018). The prepared gas mixture flows through a 15-meter stainless steel heating coil where the gases are heated to the experimental temperature (600 K, 400 K, or 300 K), and then into a stainless-steel reaction chamber where they are exposed to UV photons, inducing chemical processes that lead to the formation of new gas phase products and solid particles. The UV light source is a UV lamp (HHeLM-L, Resonance LTD.). The lamp was set to produce continuum UV photons from 110 nm to 400 nm. The total UV flux of the lamp is about 3×10^{15} photons/(sr*s), and the VUV and UV output spectrum can be found at www.resonance.on.ca. Lamps with similar wavelength range and flux are used for simulating photochemistry in atmosphere of early Earth and Titan (see e.g., Trainer et al. 2006, 2012; Sebree et al. 2014; Hörst et al. 2018b). Although the photons in this wavelength range are not sufficiently energetic to directly dissociate very stable molecules such as N_2 or CO, previous studies show that incorporation of nitrogen in organic products produced from N_2/CH_4 mixtures that were irradiated with similar UV lamps, suggesting an unknown photochemical process is occurring to incorporate N into the molecular structure of the aerosol (Hodyss et al. 2011, Trainer et al. 2012). The organics produced in these experiments could be the source for life to arise (e.g., Miller 1953; Sagan & Khare 1971; Trainer et al. 2006, 2012; Hörst et al. 2012, 2018b), since many nitrogenous molecules, such as amino acids and nucleobases, are building blocks of life.

The gases flow continuously under UV irradiation for 72 hr and solid particles (if produced in the experiment) are deposited on the wall of the reaction chamber and quartz substrate discs (purchased from Ted Pella, Inc., made from high quality fused quartz and optical-grade clear polished on both sides) which were placed at the bottom of the chamber. We ran our AC glow discharge (plasma) experiments for 72 hr under the same conditions (He et al. 2018, Hörst et al. 2018a), thus we followed the same procedure here for comparison. The chamber is further kept under vacuum for 48 hr to remove the

volatile components, and then transferred to a dry (<0.1 ppm H_2O), oxygen free (<0.1 ppm O_2) N_2 glove box (Inert Technology Inc., I-lab 2GB) where the quartz discs containing deposited particles are retrieved under dry N_2 atmosphere. The discs are kept in the glove box and wrapped in foil to avoid exposure to air and light, respectively.

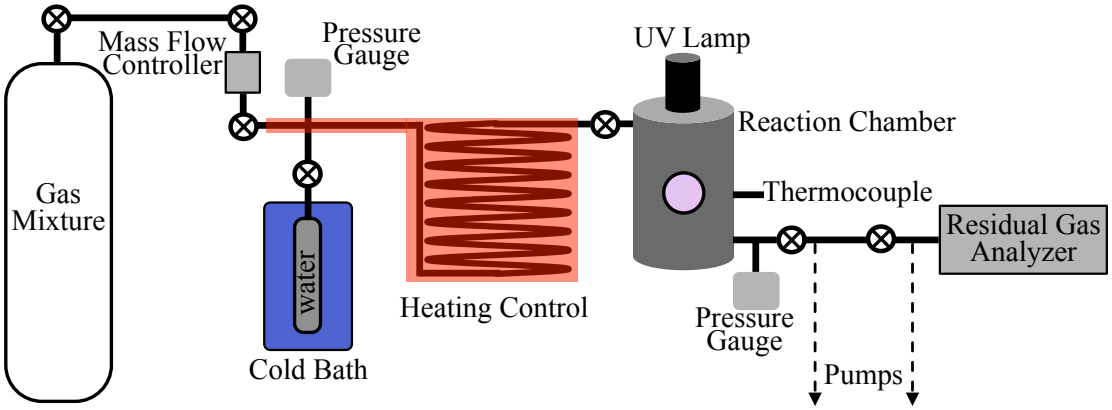

Figure 1. Schematic of the experimental setup used for this work. Due to the large variety of gases used for these experiments, the schematic shown here provides a general idea of the setup. The detailed procedure was discussed in He et al. (2018).

Table 1. Summary of initial gas mixtures. Our experimental phase space spans 100× to 10000× solar metallicity and temperatures ranging from 300 to 600 K with compositions calculated from thermochemical equilibrium at a stratospheric pressure of 1 mbar.

	100×	1000×	10000×
600 K	72.0% H_2 6.3% H_2O 3.4% CH_4 18.3% He	42.0% H_2 20.0% CO_2 16.0% H_2O 5.1% N_2 1.9% CO 1.7% CH_4 13.3% He	66.0% CO_2 12.0% N_2 8.6% H_2 5.9% H_2O 3.4% CO 4.1% He
400 K	70.0% H_2 8.3% H_2O 4.5% CH_4 17.2% He	56.0% H_2O 11.0% CH_4 10.0% CO_2 6.4% N_2 1.9% H_2 14.7% He	67.0% CO_2 15.0% H_2O 13.0% N_2 5.0% He
300 K	68.6% H_2 8.4% H_2O	66.0% H_2O 6.6% CH_4	67.3% CO_2 15.6% H_2O

4.5% CH_4	6.5% N_2	13.0% N_2
1.2% NH_3	4.9% CO_2	4.1% He
17.3% He	16.0% He	

2.2. Atomic Force Microscopy (AFM) Measurement

Several different techniques have been used to measure the particle sizes of Titan haze analogs prepared in laboratories, including Scanning Mobility Particle Sizer (SMPS, see e.g., Trainer et al. 2006; Hörst & Tolbert 2013 & 2014), Scanning Electron Microscopy (SEM, see e.g., Szopa et al. 2006, Hadamcik et al. 2009, Sciamma-O'Brien et al. 2017), Transmission Electron Microscopy (TEM, see e.g., Trainer et al. 2006, Curtis et al. 2008), and AFM (Hasenkopf et al. 2011). Here we use AFM because it can image the original sample surface without requiring an additional coating or exposing the sample to electron radiation.

The surface morphology of the particles on the quartz discs is examined using a Bruker Dimension 3100 atomic force microscope (Bruker Nano, Santa Barbara, CA). The tip (silicon probe, Tap300-G, Ted Pella, Inc) and the setting (tapping mode) for the measurement are the same as our previous study (He et al. 2018). The tip radius is less than 10 nm and conical angle at the apex is less than 20°. The AFM images are acquired by scanning the sample under ambient laboratory conditions (298 K) at a scan rate of 1.5 Hz.

3. RESULTS AND DISCUSSION

3.1. Photochemical Haze Formation and AFM Images of the Particles

In our plasma experiments, all simulated atmospheres produced particles, but the particle production rate varied substantially, as high as 10 mg/hr for the cooler (300 and 400 K) 1000× metallicity experiments (Hörst et al. 2018a). For our current UV experiments, no particles were observed by visual inspection on the walls of the chamber after 72 hr flow under UV irradiation. No obvious difference between the quartz discs from the experiments and the blank quartz disc (not exposed to UV or experimental gas mixtures) could be visually observed. This suggests that the production rates must be very low even

if the photochemical processes generate haze particles. Compared to the clear discs from current UV experiments, our previous plasma experiments for the same gas mixtures produced many more particles and formed colorful films (He et al. 2018). It is not surprising since the haze production rates from UV experiments are usually lower than those from plasma experiments (Peng et al. 2013, Hörst et al. 2018b).

Since it is difficult to determine whether or not haze particles are formed by visual examination, we observed the discs under AFM. Figure 2 shows AFM images of these discs and a clean blank quartz disc, displaying 1 μm x 1 μm scanning area for each one. AFM image displays that the blank disc has a smooth, clean surface. Compared to the blank disc, spherical particles are observed on the discs from all nine experiments, indicating that haze particles are produced from photochemical processes in all nine diverse atmospheres. Figure 2 shows that the number and size of the particles from these experiments have great variations with the different gas mixtures at different temperature. There are numerous small particles produced from the 400 K experiments, while the 600K and 300 K experiments generate fewer particles with broader size range. For all compositions, the 400 K experiments produced the smallest particles and the 300 K experiments typically produced the largest particles, despite the fact that the initial gas compositions were very similar at these two temperatures. The 600 K experiments had particle sizes intermediate to those at 300 and 400 K. From the AFM images, the diameter of the particle can be determined from its projection on the x-y plane. This method gives an accurate result (measurement errors are less than 3 nm) in the size range we measured (Villarrubia 1997, Klapetek et al. 2011). For the 600 K experiments, the particles (diameter 20 to 110 nm) are sparsely spread on the discs, while for the 400 K experiments, numerous small particles (diameter 15 to 60 nm) are densely deposited on the quartz disc. The 300 K cases produce particles with wider size range (diameter 35 to 190 nm).

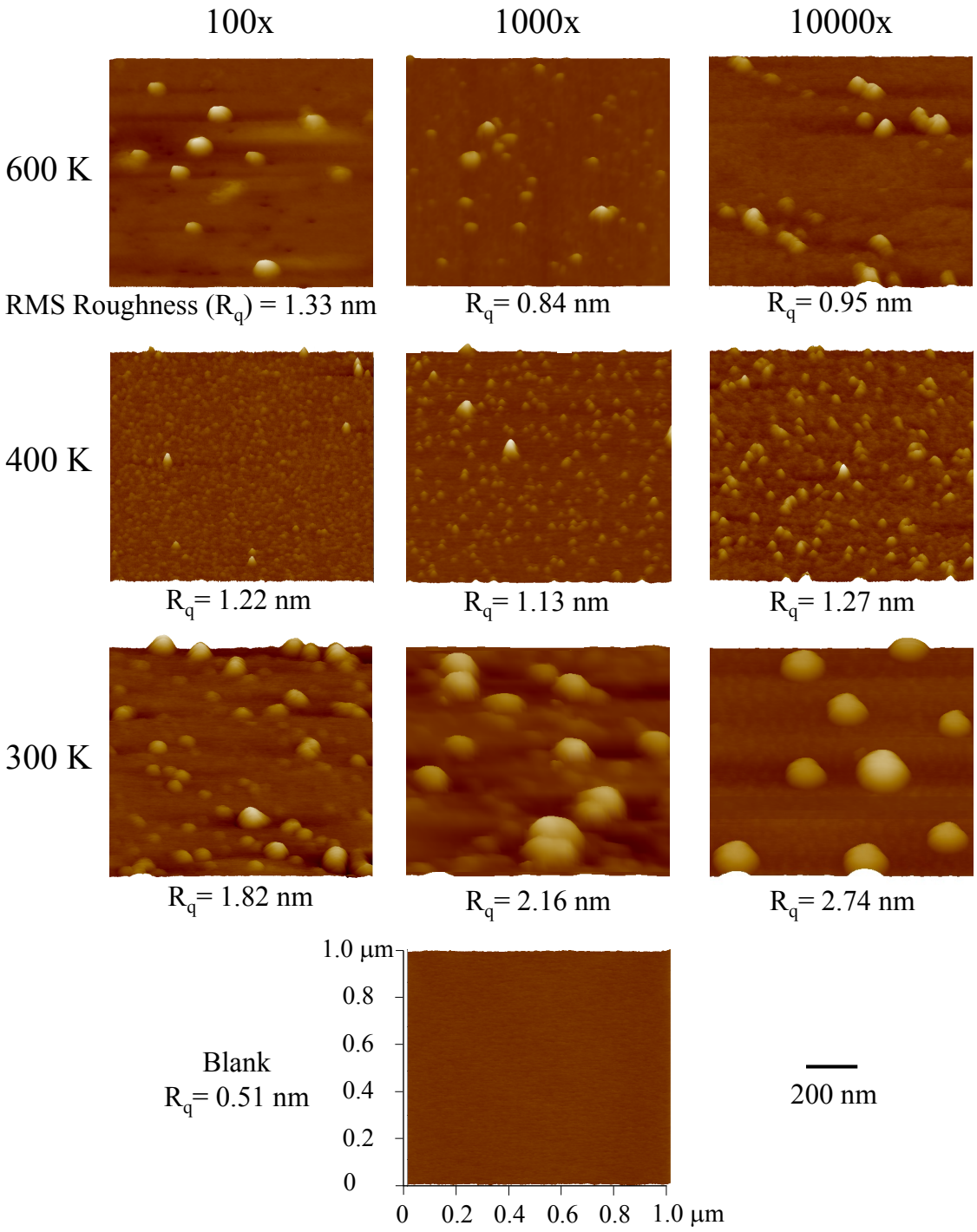

Figure 2. AFM 3D images of the particles deposited on quartz discs. Scan area is 1 µm×1 µm. Blank is the AFM image of a clean blank quartz disc. The height scale of the images is 50 nm for the 300 K and 600 K experiments, 20 nm for the 400 K experiments to better show the small particles, and also 20 nm for the blank disc. The root mean square (RMS) roughness (R_q) of the film (1 µm×1 µm) is shown under the images. The roughness (< 3 nm) indicates the films are smooth.

As shown in the AFM images (Figure 2), the haze particles are produced from photochemical processes in all nine diverse atmospheres. However, the production rates are so low in these UV experiments, and there is not enough solid produced to collect and weigh. Therefore, it is difficult to compare the production rates of these experiments. Due to the low production rate, the particles are assumed to be deposited as single layer on the quartz disc, as shown in Figure 2. Very few or no aggregates are observed in the AFM images, indicating that most of the haze particles produced in the phase space we investigated here are monomers. The roughness (< 3 nm) indicates the films are smooth, supporting single layer of monomers on the discs. The general size range from all nine experiments is from 15 nm to 190 nm, which is similar to that (20 nm to 180 nm) from our previous plasma experiments at the same conditions. This is a relatively narrow range, considering the huge differences in the gas compositions, temperatures, and energy sources. It could imply some similarity in the nucleation and growth mechanism. For instance, the same flow rate (10 sccm) and the pressure range (few Torr) could be responsible for the narrow size range. However, it is very difficult to address the detailed mechanism due to the complexity of the physics and chemistry in these gas mixtures.

3.2. Particle Size Distributions

The general size ranges are similar for both UV and plasma experiments, but the particle size range for each particular case (temperature by metallicity) is distinct. In order to better reveal the particle size distribution, we analyzed the particle size in a larger scanning area (10 μm x 10 μm) for each case, and plotted the percentage of particles ($N/N_{total}\times100\%$) in 5 nm bins (Figure 3). As shown in Figure 3, the haze particles are bigger and have a wider range at 300 K; the particles formed from the 100× metallicity mixture are between 35 nm and 125 nm in diameter, those from the 1000× mixture are between 60 nm and 190 nm, while those from the 10000× mixture vary from 80 nm to 130 nm. In contrast, the haze particles formed at 400 K are smaller but more uniform: 15 nm to 50 nm for the 100× mixture, 20 nm to 60 nm for the 1000× mixture, and 25 nm to 60 nm for the 10000× mixture. Compared to the 300 K and 400 K result, the particles produced at 600 K appear in the middle for both the average size and the size distribution range: 60 nm to 110 nm for the 100× mixture, 20 nm to 80 nm for the 1000× mixture, and

30 nm to 90 nm for the 10000× mixture. Unlike the plasma experiments (He et al. 2018), no bimodal size distribution is noticed in current UV experiments (Figure 3), confirming that most of the particles are monomers.

The experimental matrix varied in temperature and metallicity and all 9 initial gas mixtures are compositionally distinct. Previous studies showed that the initial gas composition has an important impact on the particle size of Titan haze analogs (Hadamcik et al. 2009, Hörst & Tolbert 2014, Sciamma-O'Brien et al. 2017). However, our results suggest that the particle sizes are also temperature dependent. The temperature dependence of the particle size is more obvious for the particles formed in the 300 K and 400 K experiments, since the compositions do not vary much between the 300 K and 400 K experiments. Such temperature dependence was not observed in our previous plasma experiments, indicating that the temperature could play an important role in the photochemical formation of the haze particles. The temperature directly affects the energy levels, movements, and collisions of different molecules, and the vapor pressure of newly formed species, thus impacting the reaction rate coefficient, the formation and the nucleation of the particles. In the 400 K experiments, there might be more nucleation centers that induce the formation of a large number of small and uniform particles. In contrast, heterogeneous reactions on fewer nucleation centers could lead to the broader size range in 300 K and 600 K experiments, as observed in the plasma experiments (He et al. 2018). However, the reactions and the resulting compositions for each case could be totally different, so further comprehensive investigations are required to fully understand how the temperature affect the particle size in different gas mixtures.

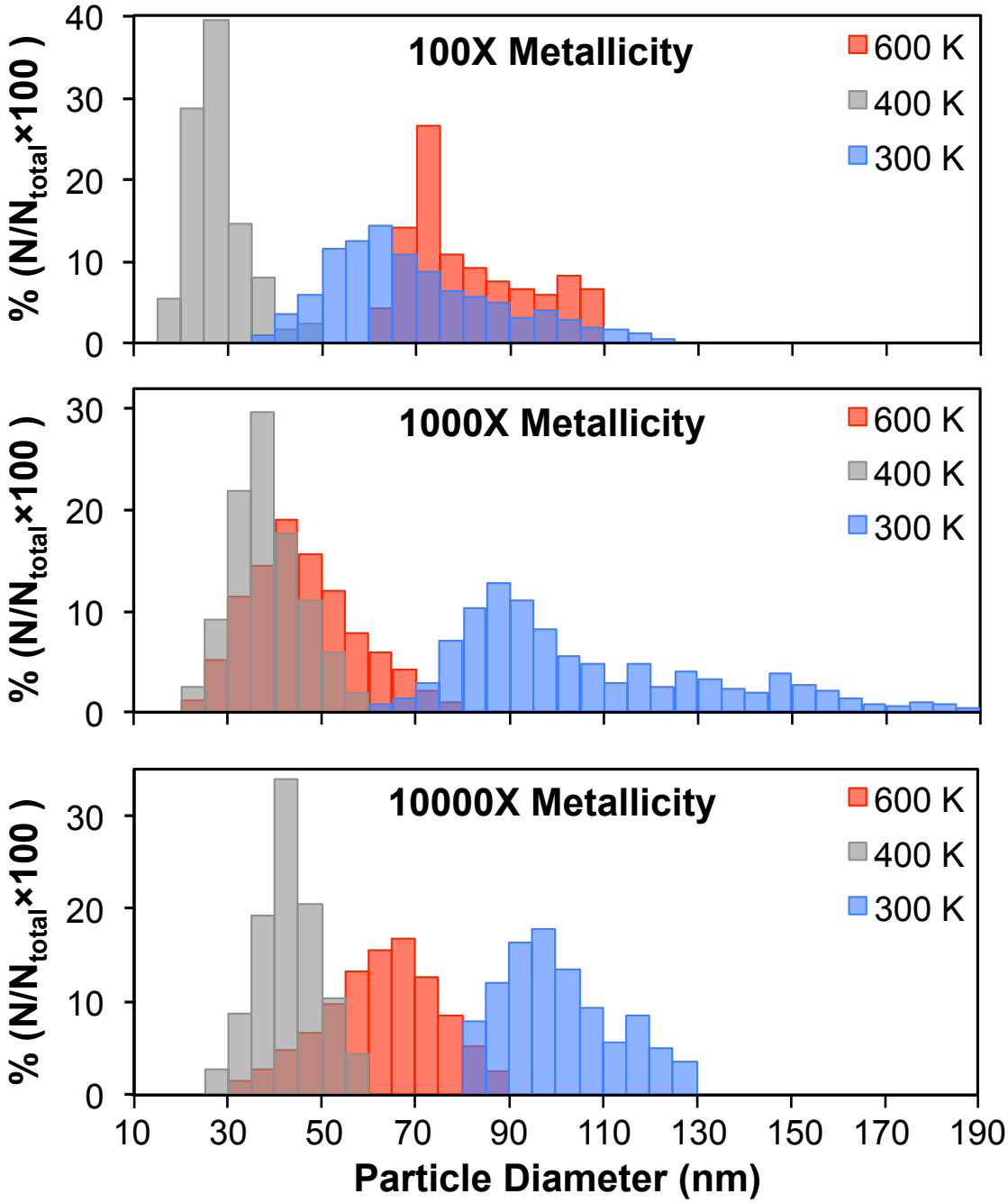

Figure 3. Size distribution of the haze particles formed in the nine experiments. The haze particles formed at 300 K are bigger and in wider range, while those at 400 K are smaller but more uniform; the particles produced at 600 K appear in the middle for both the average size and the size distribution range compared to those at 300 K and 400 K.

3.2. Haze Production Rates

If we assume the size distribution and surface density of particles on the inside wall of the chamber are the same as that on the quartz disc, we can calculate the total volume (V) of

the particles based on the number and size distribution we learned from the AFM images:

$$V = \sum_{i=0}^{i} \frac{\pi}{6} D_i^3 N_i \quad (1)$$

where D_i is the median particle diameter in each bin, N_i is the number of particles in each bin over the total available surface area within the chamber.

If we assume the particle densities are the same for all the nine cases and do not change as function of size, we can calculate the total mass of the particles by giving a density equal to that of Titan tholin sample (He et al. 2017). Previous studies show that the particle density varies with the initial gas mixture (Hörst & Tolbert 2013 & 2014, He et al. 2017). Nine gas mixtures investigated here are compositionally distinct, so the particle densities for nine experiments are unlikely to be the same. Although the constant density assumption we made here may not be correct, it allows us to estimate the production rate, and to compare to those from other experiments. The total mass (m) of the particles equals volume times density [ρ = 1.38 g cm^{-3}, average density of Titan tholin samples from previous study (He et al. 2017)].

The total volume and mass of the haze particles produced in the nine experiments are plotted in Figure 4, and the production rates are listed in Table 2. The production rates of our previous experiments (He et al. 2018, Hörst et al. 2018a) are also included in Table 2. For those plasma experiments that did not produce enough solid particles to collect and weigh, the production rates are determined by the method described above. As shown in Table 2, the production rates of the UV experiments are lower than those of the plasma experiments, except the 100× experiments at 300 K that we could not compare directly (since the production rates calculated for the 100× plasma experiment at 300 K is a lower limit). Figure 4 and Table 2 shows that the 1000× experiment at 300 K has the highest production rate (0.060 mg/hr) among the nine UV experiments. Interestingly, the 1000× plasma experiment at 300 K also has the highest production rate, although it has much higher rate (10.43 mg/hr). The 1000× experiments at 300 K have the highest haze production rate for both energy sources, indicating that we expect small, cool planets with high metallicity atmospheres to have substantial haze production. As shown in

Figure 4 and Table 2, the haze production rate in the UV experiments decrease as the temperature increases for each metallicity group, except the 10000× experiments that have similar production rates at 400 K and 600 K. This temperature dependence could be related to the vapor pressure of newly-formed species. The vapor pressure of any substance increases as the temperature increases. At lower temperature (300 K), the newly-formed species have lower vapor pressure and tend to condense and/or nucleate, generating more particles; at higher temperature (400 K and 600 K), the vapor pressure of the newly-formed species increase, and these species are more likely to stay in gas phase and be removed from the system. Further compositional analysis of both the gas phase and solid phase products are required to verify this idea.

The nine experiments started from different gas mixtures, but all led to the formation of haze particles, demonstrating that there are multiple photochemical pathways for organic haze formation. For the 100× and 1000× experiments, CH_4 provides the carbon source for the organic haze, but the 10000× experiments have no CH_4 at all. For the 10000× cases, both current UV experiments and our previous plasma experiments (He et al. 2018) generate organic haze particles. The haze formation in the absence of methane indicates other carbon sources for the organics, such as CO and CO_2. Previous studies have shown that a variety of organic compounds can be produced in the gas mixture of $CO/N_2/H_2O$ or $CO_2/N_2/H_2O$ under UV (or plasma) irradiation (See eg., Bar-Nun & Chang 1983, Plankensteiner et al. 2004, Cleaves et al. 2008). Our result demonstrates that CO and CO_2 could provide carbon source for organic hazes, and CH_4 is not necessarily required. It is important to note that the production rates are not simply a function of carbon abundance. Many factors, such as the reducing/oxidizing environment of the system, the absorption cross-sections of different reaction species, and the temperature, can affect the photochemical haze production. In addition, all 9 gas mixtures investigated are compositionally distinct. Therefore, further work is necessary to understand the complex photochemical processes leading to the formation of organic hazes.

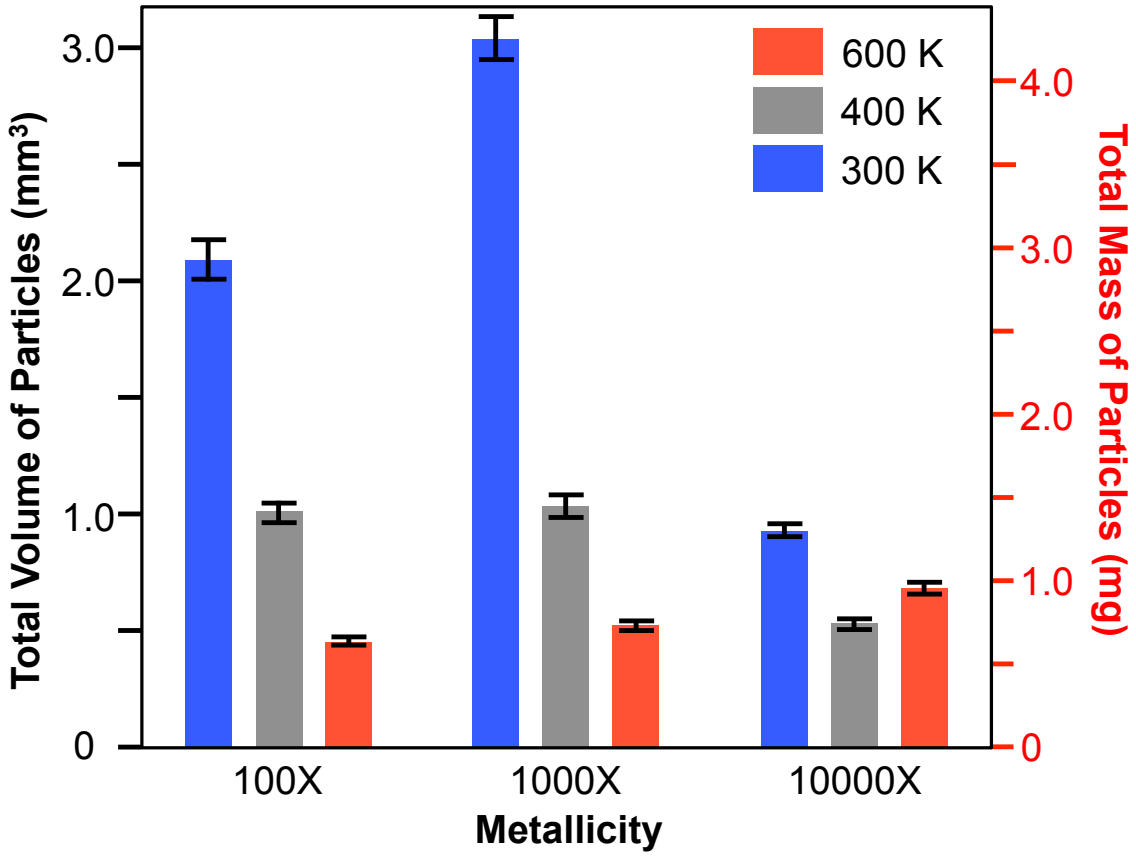

Figure 4. The total volume and the total mass of the particles produced in the nine experiments. We assume a fixed particle density (ρ = 1.38 g cm^{-3}) to calculate total mass of the particles (the right axis). The total volume or the total mass of the particles produced in each metallicity group decrease as the temperature increases, except the 10000× experiments that have similar production rates at 400 K and 600 K. The 1000× experiment at 300 K has the highest production rate among the nine UV experiments.

Table 2. Production rates (mg h^{-1}) of the haze particles produced in our previous plasma experiments (Hörst et al. 2017) and current UV experiments

	100x		1000x		10000x	
	Plasma	UV	Plasma	UV	Plasma	UV
600 K	0.04	0.008*	0.15	0.010*	0.31	0.013*
400 K	0.25	0.019*	10.00	0.021*	0.013*	0.010*
300 K	>0.016*	0.041*	10.43	0.060*	0.052*	0.018*

"*" indicates that the experiment did not produce enough solid particles to collect and weigh, and the production rate is determined by the method described in the text. The method applies to experiments with single layer of particles. ">" indicates a production rate lower limit since the AFM image (He et al. 2018) suggests there might be multiple layers of particles deposited on the substrate.

Due to the complexities of real atmospheres compared to the laboratory, it is challenging to convert laboratory production rates into actual planetary haze production rates, but our

approach here provides insights into which regions of temperature and metallicity phase space may result in photochemical haze production. Our result shows that photochemical hazes are produced in a variety of atmospheres, suggesting that haze layers could be more ubiquitous in exoplanet atmospheres than we thought. It should be noted that some minor components that are excluded in our initial gas mixtures (such as sulfur species) might be important for haze formation in exoplanet atmospheres (Zahnle et al. 2016, Gao et al. 2017). The photochemical organic haze formation in exoplanet atmospheres could affect the habitability of the planet in two aspects. First, the photochemical haze could provide the organic materials prebiotically for life to arise, like that on the early Earth. Second, haze particles can interact with radiation, such as scattering and absorption, thus influencing the energy budget and the atmospheric and surface temperature of the exoplanets and their potential habitability.

Our study also provides constraints on the particle sizes of the photochemical hazes. The size distribution of the haze particles varies with metallicity and temperature. The haze particles of different sizes will scatter light differently, and thus affect the thermal structure of the exoplanet atmospheres. However, very little information is known about particle sizes in exoplanet atmospheres; wide size ranges, from 5 nm to 10,000 nm, are used in exoplanet atmospheric models (see e.g., Howe & Burrows 2012, Arney et al. 2016, Gao et al. 2017). Although a variety of models have been tried to constrain particle sizes, the results are not satisfactory. For example, several studies attempted to reproduce the featureless transit spectrum of GJ1214b, where we see strong evidence for aerosols, but these studies did not reach an agreement on the particle sizes: One study (Morley et al. 2015) showed that a range of particles (10 nm to 300 nm) can create featureless transmission spectra; while the particle radii are around 500 nm from another study (Charnay et al. 2015). The size range (15 nm to 190 nm) from our current UV experiments is comparable to that (20 nm to 180 nm) from previous plasma experiments (He et al. 2018). The particles produced in both types of experiments fall within the size range discussed by Morley et al. (2015), suggesting that small particles are more likely to form in the atmosphere of GJ1214b. The small particles lie in the Rayleigh scattering regime for visible and infrared (IR) photons, and will scatter short wavelengths more efficiently. The haze particles in this regime would have a great impact on the geometric

albedo of the exoplanet in visible and near IR regions (0.4 μm to 1.0 μm) (McCullough et al. 2014, Morley et al. 2015, Sing et al. 2016, Gao et al. 2017), which could influence the detectability of directly imaged exoplanets by the Coronagraph Instrument on the Wide-Field Infrared Survey Telescope (WFIRST) (Spergel et al. 2015). To fully understand the effect of the haze particles on observations, further study on their optical, thermal, and compositional properties are required.

4. CONCLUSIONS

We investigated the photochemical haze formation in a range of planetary atmospheres by conducting laboratory experimental simulations with the PHAZER chamber (He et al. 2017), and observed the particle sizes using AFM. Our result shows that photochemical hazes are produced in all nine UV experiments, and the haze production rates appear to be temperature dependent: the particles produced in each metallicity group decrease as the temperature increases. The AFM images demonstrate that the particle size (15 nm to 190 nm) varies with temperature and metallicity. For all compositions, the particles formed at 300K are the largest and those formed at 400 K are the smallest particles, despite the fact that the initial gas compositions were very similar at these two temperatures. The particles formed at 600 K are intermediate. The presence of haze particles significantly affects atmospheric temperature structures and could provide organic material to the surface of a planet, thereby impacting its habitability. The result from our first experimental simulations with UV radiation provides critical inputs for modeling the atmospheres of exoplanets, and valuable laboratory data for future observations with facilities such as TESS, JWST, and WFIRST.

This work was supported by the NASA Exoplanets Research Program Grant NNX16AB45G. C.H. was supported by the Morton K. and Jane Blaustein Foundation.

REFERENCES

Arney, G., Domagal-Goldman S. D., Meadows, V. S., Wolf, E. T., Schwieterman, E., Charnay, B. Claire, M., Hébrard, E., Trainer, M. G., 2016, AsBio, 16, 873

Bar-Nun, A. & Chang, S. 1983, JGR: Oceans, 88, 6662

Borucki, W. J., Koch, D. G., Basri, G. et al. 2011, ApJ, 736, 19

Charnay, B., Meadows, V., Leconte, J., Misra, A. 2015, APJL, 813, L1

Cleaves, H. J., Chalmers, J. H., Lazcano, A., Miller, S. L., Bada, J. L. 2008, OLEB, 38, 105

Curtis, D. B., Hatch, C. D., Hasenkopf, C. A., et al. 2008, Icar, 195, 792

Dragomir, D., Benneke, B., Pearson, K. A., et al. 2015, ApJ, 814, 102

Elkins-Tanton, L. T. & Seager, S. 2008, ApJ, 685, 1237

France, K., Froning, C. S., Linsky, J. L., et al. 2013 ApJ, 763, 149

Fressin, F., Torres, G., Charbonneau, D., et al. 2013, ApJ, 766, 81

Gao, P., Marley, M. S., Zahnle, K., Robinson, T. D., Lewis, N. K. 2017, AJ, 153, 139

Hadamcik, E., Renard, J.-B., Alcouffe, G., Cernogora, G., Levasseur-Regourd, A. C., Szopa, C. 2009, PSS, 57, 1631

Hasenkopf, C. A., Freedman, M. A., Beaver, M. R., Toon, O. B., Tolbert, M. A. 2011, AsBio, 11, 135

He, C., Hörst, S. M., Lewis, N. K., et al. 2018, ApJL, under review

He, C., Hörst, S. M., Riemer, S., Sebree, J. A., et al. 2017, APJL, 841, L31

Hodyss, R., Howard, H. R., Johnson, P. V., Goguen, J. D., Kanik, I. 2011, Icar, 214, 748

Hörst, S. M., He, C., Lewis, N. K., et al. 2018, Nat. Astron., accepted, arXiv:1801.06512

Hörst, S. M., Yelle, R. V., Buch, A., et al. 2012, AsBio, 12, 809

Hörst, S. M. & Tolbert, M. A. 2013, ApJL, 770, L10

Hörst, S. M. & Tolbert, M. A. 2014, ApJ, 781, 53

Hörst, S. M., Yoon, Y. H., Ugelow, M. S., et al. 2017, Icar, 301, 136

Howe, A. R. & Burrows, A. S. 2012, ApJ, 756, 176

Hu, R. & Seager, S. 2014, ApJ, 784, 63

Ito, Y., Ikoma, M., Kawahara, H., Nagahara, H., Kawashima, Y., Nakamoto, T. 2015, ApJ, 801, 144

Klapetek, P., Valtr, M., Nečas, D., Salyk, O., Dzik, P. 2011, NRL, 6, 514

Knutson, H. A., Benneke, B., Deming, D., & Homeier, D. 2014, Nature, 505, 66

Knutson, H. A., Dragomir, D., Kreidberg, L., et al. 2014, ApJ, 794, 155

Kreidberg, L., Bean, J. L., Désert, J.-M., et al. 2014, Nature, 505, 69

McCullough, P. R., Crouzet, N., Deming, D., Madhusudhan, N. 2014, ApJ, 791, 55

Miller, S. L. 1953, Science, 117, 528

Miller-Ricci, E., Seager, S., Sasselov, D. 2009, ApJ, 690, 1056

Marley, M. S., Ackerman, A. S., Cuzzi, J. N., Kitzmann, D. 2013, in Comparative Climatology of Terrestrial Planets, ed. S. J. Mackwell et al. (Tucson, AZ: Univ. Arizona Press), 367

Morley, C. V., Fortney, J. J., Marley, M. S., et al. 2015, ApJ, 815, 110

Moses, J. I., Line, M. R., Visscher, C., et al. 2013, ApJ, 777, 34

Peng, Z., Gautier, T., Carrasco, N., et al., 2013, JGRE, 118, 778

Plankensteiner, K., Reiner, H., Schranz, B., Rode, B. M. 2004, Angew Chem Int Ed, 43, 1886

Sagan, C. & Khare, B. N. 1971, Science, 173, 417

Schaefer, L., Lodders, K., Fegley, B., JR. 2012, ApJ, 755, 41

Sciamma-O'Briena, E., Upton, K. T., Salama F. 2017, Icar, 289, 214

Sebree, J. A., Trainer, M. G., Loeffler, M. J., Anderson, C. M. 2014, Icar, 236, 146

Sing, D. K., Fortney. J. J., Nikolov, N., et al. 2016, Nature, 529, 59

Spergel, D., Gehrels, N., Baltay, C., et al. 2015, arXiv:1503.03757v2

Sullivan, P. W., Winn, J. N., Berta-Thompson, Z. K., et al. 2015, ApJ, 809, 77

Szopa, C., Cernogora, G., Boufendi, L., Correia, J. J., Coll, P. 2006, PSS, 54, 394

Trainer, M. G., Pavlov, A. A., DeWitt, H. L., et al. 2006, PNAS, 103, 18035

Trainer, M. G., Jimenez, J. L., Yung, Y. L., Toon, O. B., and Tolbert, M. A. 2012, AsBio, 12, 315

Venot, O., Hébrard, E., Agúndez, M., Decin, L., Bounaceur, R. 2015, A&A, 577, A332

Villarrubia, J. S. 1997, J Res Natl Inst Stand Technol, 102, 425

Zahnle, K., Marley, M. S., Morley, C. V., Moses, J. I. 2016, ApJ, 824, 137